Nucleon effective mass and its isovector splitting

Tuhin Malik,[1,*] C. Mondal,[2,3,†] B. K. Agrawal,[2,4,‡] J. N. De,[2,§] and S. K. Samaddar[2,‖]

[1]*Department of Physics, BITS-Pilani, K. K. Birla Goa Campus, Goa 403726, India*

[2]*Saha Institute of Nuclear Physics, 1/AF Bidhannagar, Kolkata 700064, India*

[3]*Departament de Física Quàntica i Astrofísica and Institut de Ciències del Cosmos (ICCUB), Facultat de Física,*
Universitat de Barcelona, Martí i Franquès 1, E-08028 Barcelona, Spain

[4]*Homi Bhabha National Institute, Anushakti Nagar, Mumbai 400094, India*

Using an energy density functional (EDF) based on the thermodynamic Gibbs-Duhem relation, found equivalent to the standard Skyrme EDF for infinite nuclear matter, it is demonstrated that the parameters of this EDF are not uniquely determined from the fit of the empirical and theoretical data related to nuclear matter. This prevents an unambiguous determination of the nucleon effective mass ($\frac{m_0^*}{m}$) and its isovector splitting (Δm_0^*). Complementary information from dipole polarizability of atomic nuclei helps in removing this ambiguity and plausible values of $\frac{m_0^*}{m}$ and Δm_0^* can be arrived at. Presently considered fit data on infinite nuclear matter and dipole polarizability of finite nuclei yield $\frac{m_0^*}{m} = 0.68 \pm 0.04$ and $\Delta m_0^* = (-0.20 \pm 0.09)\delta$. This EDF is consistent with the constraint on the maximum mass of the neutron star.

I. INTRODUCTION

The nucleon effective mass is a measure of the mobility of the nucleon in a nuclear medium. It is defined as $d\epsilon/dp = p/m^*$, where m^* is the effective nucleon mass, ϵ the energy per nucleon in the system, and p is the magnitude of the nucleon momentum. For a homogeneous system of density ρ, $m^*(\rho)$ is defined at the Fermi surface. In isospin asymmetric nuclear matter, the neutrons and protons may feel different single-particle potentials. This may result in a difference in their mobility. The (neutron, proton) effective masses (m_n^*, m_p^*) may then be different. The isospin-splitted effective mass is defined as $\Delta m^* = (m_n^* - m_p^*)/m$, where m is the bare mass of the nucleon. The small difference between the bare neutron and the bare proton mass is neglected. There exist different kinds of nucleon effective masses in relativistic [1,2] and non-relativistic approaches [3,4], we confine ourselves specifically to a non-relativistic description. Furthermore, only that part of the mass renormalization coming from the momentum dependence of the nucleon-nucleon interaction is in focus here. The energy-mass component emanating from the coupling of the nucleon effective mass with the dynamical vibration [5,6] of the single-particle potential is left out.

Attempts have been made in the last few decades to arrive at an acceptable value for the nucleon effective mass $m^*(\rho_0)(= m_0^*)$ at the saturation density ρ_0 of symmetric nuclear matter (SNM), but a clear consensus still seems to be missing. Energy density functionals (EDF), many in the Skyrme framework, designed to effectively reproduce various empirical properties of nuclear matter and finite nuclei yield values of m_0^*/m in the range 0.6–1.0 [7–10]. Many-body calculations, irrespective of their level of sophistication give $m_0^*/m \sim 0.8 \pm 0.1$ [11–13]. Analysis of isoscalar giant quadrupole resonances (ISGQR) [14–17] predicts a similar value ($\sim 0.85 \pm 0.1$), but the analysis is not model independent. Optical model analysis of nucleon-nucleus scattering, on the other hand, yields a value of the effective mass somewhat less, $m_0^*/m \sim 0.65 \pm 0.06$ [18].

The isovector sector of the nuclear interaction is mired with large uncertainty. The symmetry energy coefficient, its density derivatives of different orders and the isovector splitting of the nucleon effective mass offer a window to have a close glimpse on the nature of this part of the interaction. The isovector mass splitting is of profound importance in addressing many key problems in nuclear physics, astrophysics and even cosmology. It is critical for understanding transport and thermal properties of asymmetric nuclear matter [19–22], for neutrino opacities in neutron star matter [23,24], for locating the drip lines [25] in the nuclear mass table. It has also a crucial role to play in understanding neutron/proton ratio in primordial nucleosynthesis [26] in the early universe.

Attempts have been made in recent times to have an experimental estimation of the isovector effective mass splitting Δm_0^* (the subscript refers to its value at ρ_0). From analysis of nucleon-nucleus scattering data [18] within an isospin-dependent optical model, it is found to be $(0.41 \pm 0.15)\delta$ [δ is the isospin asymmetry defined as $(\rho_n - \rho_p)/\rho$], from exploration of ISGQR and dipole polarizability [14] it goes down to $(0.27 \pm 0.15)\delta$. On the other hand, the

*tuhin.malik@gmail.com

†chiranjib.mondal@icc.ub.edu

‡bijay.agrawal@saha.ac.in

§jn.de@saha.ac.in

‖santosh.samaddar@saha.ac.in

transport-model-motivated estimates of double n/p ratio in heavy ion collisions suggest [27] a value of $\Delta m_0^* = (-0.058 \pm 0.129)\delta$. Theoretical studies based on microscopic or phenomenological approaches have also yielded varying values of Δm_0^* [28–31]. Non-relativistic Brueckner-Hartree-Fock (BHF) and relativistic Dirac-Brueckner-Hartree-Fock (DBHF) calculations [28,29] give $\Delta m_0^* > 0$ whereas Gogny-Hartree-Fock models [32–34] result in Δm_0^* positive or negative depending on the choice of the parameters defining the force. On the phenomenological side, for around 100 Skyrme EDFs, Δm_0^* comes out to be positive for about half of them, around one-third are negative and the rest are nearly zero [35]. From constraints on Skyrme EDFs provided by properties of nuclear matter [9], of doubly magic nuclei and *ab initio* calculations of low-density neutron matter, recently some "best-fit" EDFs were isolated and listed in Table I of Ref. [36]. From the parameters of these EDFs (with the values of x_1 as given in the last column of the table), the isovector-splitted effective mass can be calculated. For all of them, Δm_0^* is found to be negative ($\simeq -0.3\delta$). Both experiment and theory, however, thus far seem to weigh in favor of a positive Δm_0^*. In this conundrum, a fresher look at the nucleon effective mass, its isovector splitting and thus a closer view of the isovector sector of the nuclear interaction is called for. This article is an attempt towards this goal, finding a means to determine the values of $\frac{m_0^*}{m}$ and Δm_0^* in a subtle way.

The paper is organized as follows. In Sec. II, the elements comprising the theoretical background are reviewed. The results and discussions are presented in Sec. III. The concluding remarks are drawn in Sec. IV.

II. THEORETICAL FRAMEWORK

In an effort to find the interdependence of the different symmetry energy elements of nuclear matter, a specific EDF was recently constructed [31] structured on the thermodynamic Gibbs-Duhem relation. Built in the confines of non-relativistic mean field approximation, no specific assumption about the nuclear interaction is made in this EDF except that it is effectively two-body, quadratically momentum dependent and that it has a power-law density dependence to simulate many-body effects. Equations relevant in the present context are presented in Sec. II A, Sec. II B contains a discussion on nuclear dipole polarizability and its relation in finding some key parameters of this EDF uniquely.

A. The energy density functional

Exploiting Gibbs-Duhem relation, the energy per nucleon of asymmetric nuclear matter at a density ρ and isospin asymmetry δ can be written as [31]

$$\epsilon(\rho, \delta) = \frac{1}{\rho} \left[\sum_\tau \frac{P_{F,\tau}^2}{10m} \rho_\tau \left(3 - 2\frac{m}{m_\tau^*(\rho)} \right) \right] - V_2(\rho, \delta) + \frac{P(\rho, \delta)}{\rho}. \tag{1}$$

The index τ refers to neutron or proton, $\rho_\tau = (1 + \tau\delta)\rho/2$; $\tau = 1$ for neutrons and -1 for protons. The Fermi momentum

$P_{F,\tau} = g\rho_\tau^{1/3}$ with $g = (3\pi^2)^{1/3}\hbar$. In Eq. (1), $P(\rho, \delta)$ is the pressure of the system and $V_2(\rho, \delta)$ is the rearrangement potential. The density and isospin dependent rearrangement potential can be expanded around $\delta = 0$ and written as

$$V_2(\rho, \delta) = (a + b\delta^2 + c\delta^4 + \dots)\rho^{\tilde{\alpha}}. \tag{2}$$

If the interaction is effectively two-body, terms beyond δ^2 are zero. The density-dependent nucleon effective mass is taken as

$$\frac{m}{m_\tau^*(\rho)} = 1 + \frac{k_+}{2}\rho + \frac{k_-}{2}\rho\tau\delta. \tag{3}$$

The isovector effective mass splitting $\Delta m_0^*(= \frac{m_n^* - m_p^*}{m})$ at ρ_0 is then given by

$$\Delta m_0^* \simeq -k_- \rho_0 \left(\frac{m_0^*}{m} \right)^2 \delta, \tag{4}$$

where at the saturation density, the approximation $(m_n^*.m_p^*) \simeq (m_0^*)^2$ is used.

Since the pressure $P = \rho^2 \frac{\partial \epsilon}{\partial \rho}$, Eq. (1) can be integrated to

$$\epsilon(\rho, \delta) = \frac{3}{2}y \left[\sum_\tau (1 + \tau\delta)^{5/3} \left\{ \rho^{2/3} + \frac{1}{2}\rho^{5/3}(k_+ + k_-\tau\delta) \right\} \right] + (a + b\delta^2)\frac{\rho^{\tilde{\alpha}}}{(\tilde{\alpha} - 1)} + K(\delta)\rho, \tag{5}$$

where $y = \frac{g^2}{10m.2^{2/3}}$ and $K(\delta) = (K_1 + K_2\delta^2 + K_4\delta^4 + \cdots)$ is a constant of integration.

The expressions for the energy of SNM and pure neutron matter (PNM) and their pressures are then written as

$$\epsilon(\rho, \delta = 0) = a\frac{\rho^{\tilde{\alpha}}}{(\tilde{\alpha} - 1)} + 3y\rho^{2/3}\left(1 + \frac{1}{2}k_+\rho\right) + K_1\rho, \tag{6}$$

$$\epsilon(\rho, \delta = 1) = (a + b)\frac{\rho^{\tilde{\alpha}}}{(\tilde{\alpha} - 1)} + 3 \times 2^{2/3}y\rho^{2/3}$$
$$\times \left[1 + \frac{1}{2}(k_+ + k_-)\rho \right] + (K_1 + K_2 + K_4 + \cdots)\rho, \tag{7}$$

$$P(\rho, \delta = 0) = \frac{\tilde{\alpha}}{(\tilde{\alpha} - 1)}a\rho^{\tilde{\alpha}+1} + y\rho^{5/3}\left(2 + \frac{5}{2}k_+\rho\right) + K_1\rho^2 \tag{8}$$

$$P(\rho, \delta = 1) = \frac{\tilde{\alpha}}{(\tilde{\alpha} - 1)}(a + b)\rho^{\tilde{\alpha}+1} + 2^{2/3}y\rho^{5/3}$$
$$\times \left[2 + \frac{5}{2}(k_+ + k_-)\rho \right] + (K_1 + K_2 + K_4 + \cdots)\rho^2. \tag{9}$$

From Eq. (5), the symmetry energy coefficient $C_2(\rho)(= \frac{1}{2}\frac{\partial^2 \epsilon}{\partial \delta^2}|_{\delta=0})$ is derived as

$$C_2(\rho) = \frac{b\rho^{\tilde{\alpha}}}{(\tilde{\alpha} - 1)} + \frac{5}{3}y\rho^{2/3}\left[1 + \frac{1}{2}(k_+ + 3k_-)\rho\right] + K_2\rho. \tag{10}$$

The parameters of this EDF can be found from the best fit to the existing empirical data pertaining to nuclear matter, i.e., the pressure of symmetric nuclear matter [37–39] and of PNM in a broad density range [37,40] and also the symmetry energy in a limited density range [41–44]. In addition, the energy and pressure of low density neutron matter calculated in high precision in chiral effective field theory (N³LO) [45,46] are taken into account in the fit data. Our analysis reveals that the fit to the infinite nuclear matter data alone is unable to fix the values of the two parameters (k_+ and k_-) separately; it tends to yield a value of the sum of the parameters. Available experimental data on the dipole polarizability in a few nuclei, on the other hand, are shown to illuminate the relation of an isovector property with the difference between these said parameters (k_+ and k_-). In this paper, we use this extra information to find values of k_+ and k_-; they are measures of the nucleon effective mass and the isovector mass splitting.

Inspection of the EDF in Eq. (5), when compared with the 'standard' Skyrme functional [9] shows that there is an exact equivalence of the Skyrme functional for infinite matter with the one given by Eq. (5) provided the term $K(\delta)$ is truncated at δ^2. In subsequent analysis, we take this prescription, i.e., K_4 and higher order terms are ignored. The parameters $\tilde{\alpha}$, K_1, K_2, a, b, k_+, and k_- can then be correlated to the standard Skyrme parameters:

$$\tilde{\alpha} = \alpha + 1,$$
$$K_1 = \frac{3}{8}t_0,$$
$$K_2 = -\frac{1}{4}t_0\left(x_0 + \frac{1}{2}\right),$$
$$a = \frac{1}{16}t_3\alpha,$$
$$b = -\frac{1}{24}t_3\left(x_3 + \frac{1}{2}\right)\alpha,$$
$$k_+ = \frac{m}{\hbar^2}\left[\frac{3}{4}t_1 + \frac{5}{4}t_2 + t_2x_2\right],$$
$$k_- = \frac{m}{2\hbar^2}\left[t_2\left(x_2 + \frac{1}{2}\right) - t_1\left(x_1 + \frac{1}{2}\right)\right]. \quad (11)$$

B. The isovector mass, the energy weighted sum rule, and dipole polarizability

Equation (3) shows that the parameters k_+ and k_- can be used to define the nucleon effective mass and the isovector mass splitting. It also defines, in terms of these parameters, the isovector nucleon mass $m^*_{v,0}$, i.e., the effective mass of a proton in pure neutron matter or vice versa at ρ_0 [14]. It is given as

$$\frac{m}{m^*_{v,0}} = 1 + \frac{m}{2\hbar^2}\rho_0\Theta_V, \quad (12)$$

where

$$\Theta_V = \frac{\hbar^2}{m}(k_+ - k_-). \quad (13)$$

An added knowledge of Θ_V helps in finding k_+ and k_-. In Skyrme parametrization, the isovector parameter Θ_V is

$$\Theta_V = \left[t_1\left(1 + \frac{x_1}{2}\right) + t_2\left(1 + \frac{x_2}{2}\right)\right]. \quad (14)$$

The parameter Θ_V is related to m_1, the energy weighted sum rule (EWSR) for the dipole excitations. The kth moment of the energy weighted sum is defined as

$$m_k = \int dE E^k S(E), \quad (15)$$

where $S(E)$ is the strength function at energy E. For the isovector giant dipole resonance (IVGDR) of a nucleus with mass number A, neutron number N, and proton number Z, the EWSR can be written as [5]

$$m_1 = \frac{9}{4\pi}\frac{\hbar^2}{2m}\frac{NZ}{A}(1 + \kappa_A), \quad (16)$$

where κ_A is the polarizability enhancement factor for the nucleus in question. It is related to Θ_V as [47]

$$\kappa_A = \frac{2m}{\hbar^2}\frac{A}{4NZ}\Theta_V \times I_A, \quad (17)$$

where $I_A = \int \rho_n(r)\rho_p(r)d^3r$; $\rho_n(r)$ and $\rho_p(r)$ are the neutron and proton density distributions of the nucleus. In principle, m_1 can be found out from the experimentally determined strength function $S(E)$; it is then possible to get to a value of Θ_V provided the integral occurring in Eq. (17) is known. However, the high energy component of the strength function is plagued with 'quasi-deuteron effect' rendering the determination of m_1 or κ_A not very reliable [48,49].

It need be mentioned that experimental data for the inverse energy weighted sum m_{-1} for a few nuclei [50–53], or in other words, the nuclear dipole polarizability are available. They are related as

$$\alpha_D = \frac{8\pi e^2}{9}\int dE E^{-1}S(E) = \frac{8\pi e^2}{9}m_{-1}. \quad (18)$$

Using Eqs. (16) and (18), one can then write

$$m_1 = \frac{9}{8\pi e^2}E_x^2\alpha_D, \quad (19)$$

where the energy $E_x = (\frac{m_1}{m_{-1}})^{1/2}$ is referred to as the constrained energy [54]. To find Θ_V, values of m_1 are constructed from reasonable inputs on E_x which we discuss in the next section.

III. RESULTS AND DISCUSSIONS

In order to determine $\frac{m_0^*}{m}$ and Δm_0^*, one needs to know the values of k_+ and k_- [Eqs. (3) and (4)]. The calculations are performed in two stages. In stage 1, the seven parameters $\tilde{\alpha}$, K_1, K_2, a, b, k_+, and k_- occurring in the EDF given by Eq. (5) are obtained from optimization of the χ^2-function from a fit to all the different empirical and precision theoretical data listed in Table I. In the fitting protocol, in addition, values of three empirical nuclear constants pertaining to SNM (energy per nucleon ϵ_0, saturation density ρ_0, and incompressibility K_0) are further chosen to be constrained;

TABLE I. List of fit data [$P(\rho)$, $\epsilon_n(\rho)$, and $C_2(\rho)$ represent pressure, energy per particle, and symmetry energy, respectively] corresponding to the symmetric nuclear matter (SNMX), pure neutron matter (PNMX), and symmetry energy coefficient (SYMX) together with the range of densities in which they are determined.

	Quantity	Density region (fm^{-3})	Band/Range (MeV)	Ref.
SNM1	$P(\rho)$	0.32 to 0.74	HIC	[37]
SNM2	$P(\rho)$	0.19 to 0.33	Kaon exp	[38,39]
PNM1	$\epsilon_n(\rho)$	0.1	10.9 ± 0.5	[36]
PNM2	$\epsilon_n(\rho)$	0.03 to 0.17	N^{3}LO	[45]
PNM3	$P(\rho)$	0.32 to 0.73	HIC	[37]
PNM4	$P(\rho)$	0.03 to 0.17	N^{3}LO	[45]
SYM1	$C_2(\rho)$	0.1	24.1 ± 0.8	[55]
SYM2	$C_2(\rho)$	0.01 to 0.19	IAS,HIC	[41,43]
SYM3	$C_2(\rho)$	0.01 to 0.31	ASY-EoS	[44]

they are taken from the averages of the 'best-selected' nuclear EoS given in Ref. [9]. Their values are $\epsilon_0 = -15.88 \pm 0.24$ MeV, $\rho_0 = 0.163 \pm 0.005$ fm^{-3}, and $K_0 = 226.2 \pm 10.1$ MeV. These values refer to infinite symmetric nuclear matter, but with roots embedded to finite nuclear observables. Henceforth, these data would be referred to as 'macrodata'. This fitting protocol is seen to be incapable of yielding the values of k_+ and k_- uniquely, but gives a value of a linear combination of them (shown later). In stage 2, by fitting the 'constructed' values of m_1 [see Eq. (19)] from chosen values of E_x (discussed in Sec. III B) for the considered nuclei, we get Θ_V which is a different linear combination of k_+ and k_- as given by Eq. (13). Combining results from the two stages, unique values of k_+ and k_- are obtained. The errors pertaining to the studied observables are calculated from the curvature matrix obtained from the double derivative of χ^2-function with respect to different parameters employing the method of covariance analysis [56–58].

A. Fitting of macrodata

The macrodata (barring the ones at the saturation density) used in the fitting protocol are listed in Table I. The rows and columns are self-explanatory. The first two rows refer to pressure of SNM. They are obtained from analysis of directed and elliptic flow [37] and kaon production [38,39] in heavy ion collisions (HIC). The next four rows correspond to PNM. Its energy at a density $\rho = 0.1$ fm^{-3} is taken from the 'best-fit' Skyrme EDFs [36]. The information on the energy and pressure of low density neutron matter is taken from high precision predictions at next-to-next-to-next-to- leading order (N^{3}LO) in chiral effective field theory [45,46]. The pressure of PNM is the excess over the pressure of SNM due to symmetry energy. It is constructed theoretically with two extreme parametrizations, the soft (Asy Soft) and the stiff (Asy Stiff) symmetry energy [40]. Its values are taken from Ref. [37]. The last three rows refer to the symmetry energy coefficients $C_2(\rho)$ at the densities mentioned in the table. They come from three different sources, namely, simulation of low energy HIC in ^{112}Sn + ^{112}Sn and ^{124}Sn + ^{124}Sn [41,42],
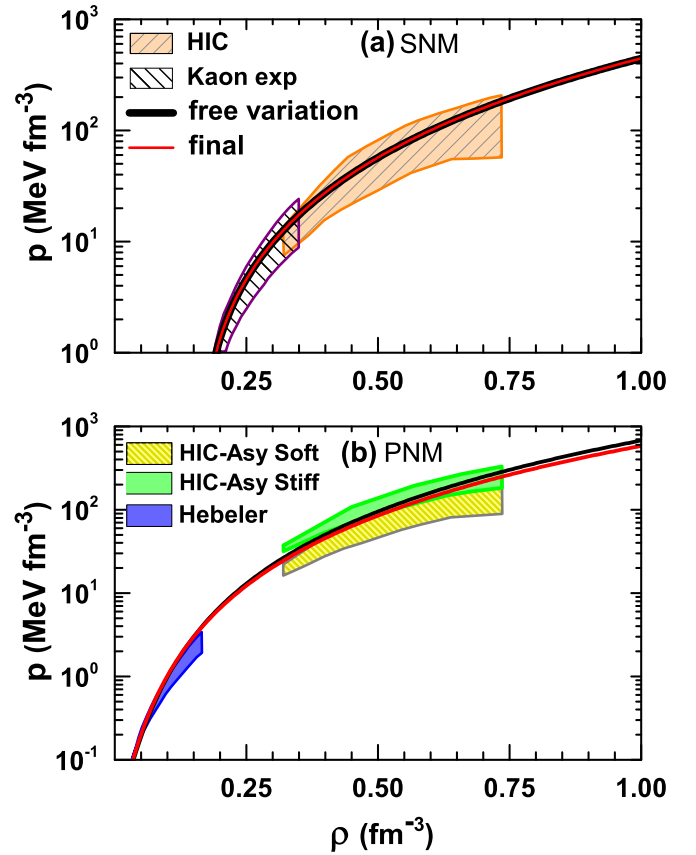

FIG. 1. The pressure $P(\rho)$ for SNM (upper panel) and PNM (lower panel) as a function of baryon density ρ for the best-fit parameters obtained from free variation of all the parameters (black lines) and for the final values of the parameters (see Table II) shown by the red line.

nuclear structure studies involving isobaric analogue states (IAS) [43] and Asy-EOS experiments at GSI [44]. In addition, the value of $C_2(\rho)$ at $\rho = 0.1$ fm^{-3} quoted from microscopic analysis of IVGDR in ^{208}Pb is taken [55] into consideration.

A free variation of all the seven parameters with the above fitting protocol yields a very shallow minimum in χ^2 corresponding to $\frac{m_0^*}{m} \simeq 1.31$ and $\Delta m_0^* \simeq -2.9\,\delta$. The fit to the empirical data is found to be very good as shown by black lines in Figs. 1 and 2. The χ^2-function is, however, found to be very flat. In order to get an insight into this flatness problem, we constrain $\tilde{\alpha}$ to a fixed value and optimize χ^2 varying the remaining six parameters. This is similar to the method adopted by Friedrich and Reinhard [59] in finding out the interaction parameters of the Skyrme EDF in their fitting protocol from their chosen data. They found their routine incapable of determining α (= $\tilde{\alpha} - 1$) and therefore had to be varied by hand to determine the remaining Skyrme parameters. We do likewise, we repeat the fitting calculations for different choices of $\tilde{\alpha}$. Each choice of $\tilde{\alpha}$ leads to a different set of EDF parameters and thus $\frac{m_0^*}{m}$. Each parameter set is found to be equally good in fitting the macrodata, an unique value of $\frac{m_0^*}{m}$ can not thus be arrived at from this fitting. We find that $\frac{\Delta m_0^*}{\delta}$ decreases with increase in $\frac{m_0^*}{m}$. The trend is found to
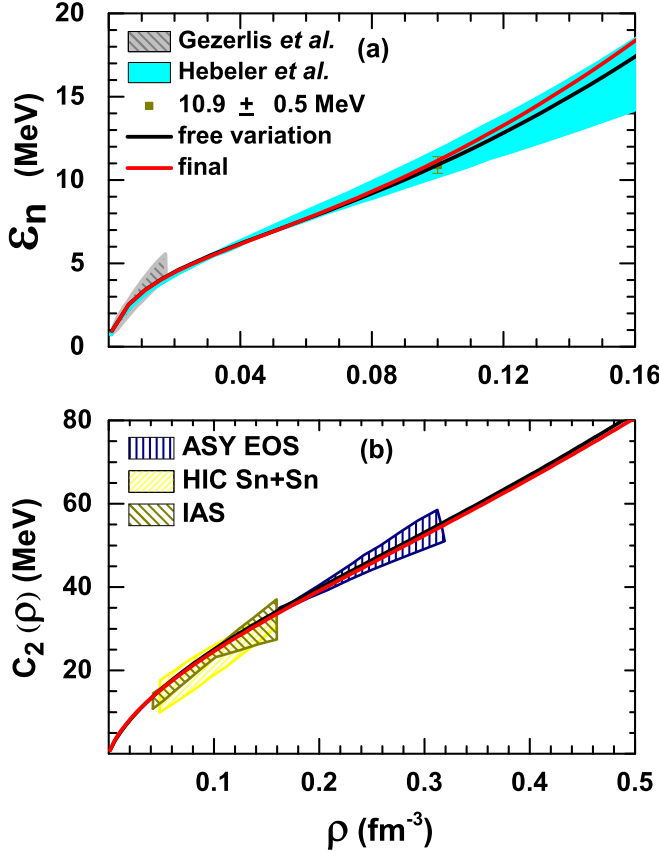
FIG. 2. The energy per neutron ϵ_n of PNM (upper panel) and symmetry energy coefficient $C_2(\rho)$ (lower panel) as a function of baryon density ρ. The black and the red lines bear the same meaning as in Fig. 1.

be almost parabolic in nature (more on this is discussed later in relation to Fig. 5).

B. Fitting of EWSR

Equations (16) and (17) show that the isovector entity Θ_V can be calculated if the EWSR sum m_1 and the integral I_A are known. From the neutron and proton densities $\rho_n(r)$ and $\rho_p(r)$ calculated in the Hartree-Fock approximation for the four nuclei viz. ^{48}Ca [50], ^{68}Ni [51], ^{120}Sn [52], and ^{208}Pb [53] (for which data on nuclear dipole polarizability are available) with the 'best-fit' Skyrme-EDF reported in Ref. [36], it is found that the integrals I_A for a particular nucleus are nearly independent of EDFs. This manifests in an extremely strong correlation (with correlation coefficient practically unity) between Θ_V and κ_A as displayed in Fig. 3. The slopes of the correlation lines are taken as measures for I_A for each nucleus; they are shown in respective panels in the figure.

Since the experimental values of m_1 are not very reliable due to the contamination from 'quasi-deuteron effect', existing data on α_D for the four nuclei can be exploited to gauge the measures of m_1 in good bounds with reasonable choice of E_x. Two choices for its values are made. For its lower value, the known peak energy E_p of the experimental IVGDR
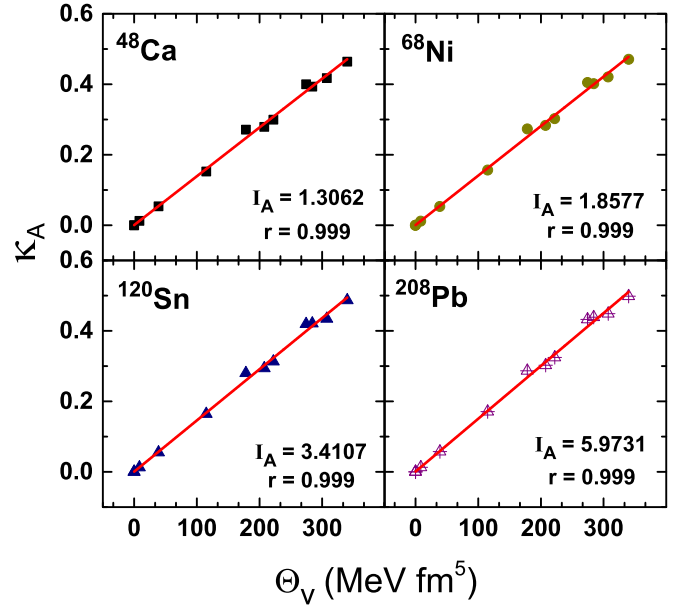

FIG. 3. The correlation of the isovector parameter Θ_V obtained from the Skyrme EDFs [36], with the calculated dipole enhancement factor κ_A for the nuclei ^{48}Ca, ^{68}Ni, ^{120}Sn, and ^{208}Pb. The corresponding values of the integrals I_A (in units of fm^{-3}) and the correlation coefficients are shown in each panel.

strength function is chosen. For the higher value, we take $E_x = 1.05 E_p$. This choice is prompted from our finding that RPA calculations with the best-fit Skyrme EDFs [36] yield E_x to be higher than E_p by $\sim$ (4–6)% for the nuclei studied. These two choices of E_x give the lower and upper bounds of m_1.

First equating E_x with E_p, the peak energy of the experimental IVGDR strength distribution, m_1 are calculated for the four nuclei from the experimentally obtained values of α_D [see Eq. (19)] which are referred to as 'calibrated' values of m_1. Using these calibrated values, the enhancement factor κ_A for the chosen nuclei are determined from Eq. (16). With the known values of I_A and so obtained κ_A are then subjected to a χ^2 minimization by varying Θ_V [Eq. (17)]. The optimized value of Θ_V is found to be $\Theta_V = 105.0$ MeV fm^5. The calculation is repeated with E_x increased by 5% above the values of E_p. The optimized value of Θ_V is now 185.0 MeV fm^5. The fitted results with the two sets of calibrated values of m_1 are shown in the upper and lower panels of Fig. 4. In both cases the fits are very good. An average value of $\Theta_V \simeq 145.0 \pm 40.0$ MeV fm^5 can be inferred from the calculations. Since Θ_V determines the difference between k_+ and k_-, its constancy demands that if k_+ increases, k_- should also increase.

Using Eqs. (3), (4), and (13), one gets

$$\frac{\Delta m_0^*}{\delta} = \left(\frac{m}{\hbar^2} \Theta_V \rho_0 - 2\frac{m}{m_0^*} + 2 \right) \left(\frac{m_0^*}{m} \right)^2. \qquad (20)$$

One finds increase in $\frac{m_0^*}{m}$ with increase in $\frac{\Delta m_0^*}{\delta}$. This is complementary to what we obtained from fitting the macrodata. As mentioned earlier, there we find that $\frac{\Delta m_0^*}{\delta}$ decreases with
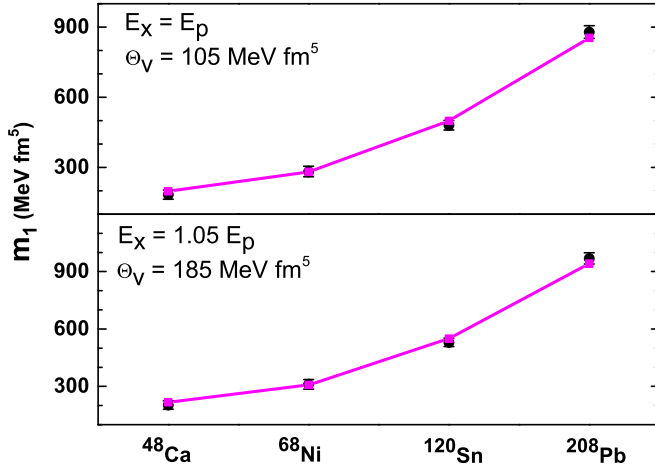
FIG. 4. The calibrated values of EWSR (m_1) displayed for the four nuclei (black squares). The upper panel shows the values with $E_x = E_p$, the lower panel displays the same with $E_x = 1.05 E_p$ (see text for details). The solid lines are drawn to show the fit with $\Theta_V = 105$ MeV fm^5 and 185 MeV fm^5, respectively.

increasing $\frac{m_0^*}{m}$ almost in a parabolic way, it can be well approximated as

$$\frac{\Delta m_0^*}{\delta} = \beta_1 + \beta_2 \left(\frac{m_0^*}{m}\right)^2 \qquad (21)$$

with $\beta_1 = 0.733 \pm 0.024$ and $\beta_2 = -2.029 \pm 0.032$. This equation can be restated as

$$(k_- + \beta_1 k_+)\rho_0 \simeq -(\beta_1 + \beta_2). \qquad (22)$$

Since β_1 and the right-hand side (r.h.s.) of this equation is positive, one finds that if k_- increases, k_+ decreases and vice versa. The opposing trends on the relation of $\frac{\Delta m_0^*}{\delta}$ on $\frac{m_0^*}{m}$ from Eqs. (21) and (20) are displayed in Fig. 5. The black dashed
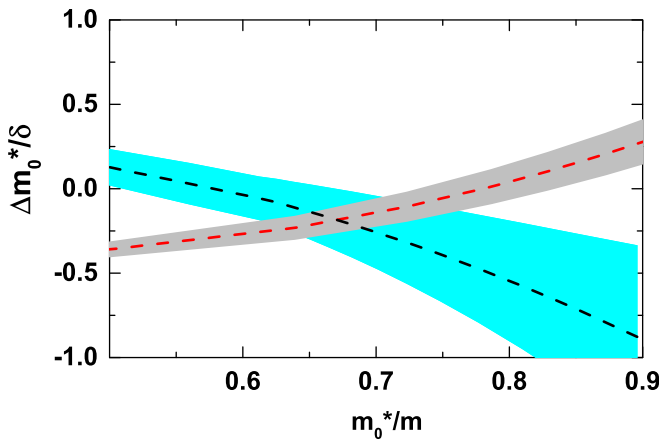

FIG. 5. The isovector effective mass-splitting as a function of nucleon effective mass. The black dashed line refers to the best fit obtained from macrodata for different values of $\tilde{\alpha}$; the red dashed line corresponds to the one obtained by satisfying Eq. (20) with $\Theta_V = 145$ MeV fm^5. The cyan and grey shades refer to the respective uncertainties.

TABLE II. The final model parameters obtained by optimizing the χ^2 function together with the uncorrelated and correlated errors (see text for details). The parameters K_1 and K_2 are in units of MeV fm^3, a and b are in MeV fm$^{3\tilde{\alpha}}$, and k_+ and k_- are in fm^3.

$\tilde{\alpha}$	K_1	K_2	a	b	k_+	k_-
1.11	-1220.21	977.94	120.03	-121.93	6.07	2.60
Unc. err.	1.16	2.38	0.15	0.33	0.10	0.15
Cor. err.	103.04	90.25	15.01	13.57	1.13	0.96

line corresponds to Eq. (21), the red dashed line corresponds to Eq. (20) with $\Theta_V = 145.0$ MeV fm^5. The lower and upper boundaries of the grey shade around the red dashed line refer to calculations with $\Theta_V = 105.0$ and 185.0 MeV fm^5, respectively. The cyan shade around the black dashed line corresponds to uncertainties involved in relation to parameter fitting.

The intersection of the dashed black and red lines yields the central values of both $\frac{m_0^*}{m}$ and $\frac{\Delta m_0^*}{\delta}$; k_+ and k_- are then known. With the constraints on ϵ_0, ρ_0, and K_0 as mentioned earlier and with known k_+ and k_-, the other parameters of the EDF are then determined from the optimization of the χ^2-fit to the macrodata given in Table I.

From the crossing of the shades as shown in Fig. 5, the values of $\frac{m_0^*}{m}$ and $\frac{\Delta m_0^*}{\delta}$ are found to be in the range 0.61 to 0.75 and -0.3 to -0.1, respectively. The final values of the parameters corresponding to the projected central values of $\frac{m_0^*}{m}$ and $\frac{\Delta m_0^*}{\delta}$ from Fig. 5 are listed in Table II. The value of $\tilde{\alpha}$ comes out to be 1.11. The uncorrelated and correlated errors of the parameters obtained within the covariance method are also presented. We see that the correlated errors are significantly higher in comparison to the uncorrelated ones which indicate the existence of strong correlations among the parameters. In Fig. 6, the correlation among the model parameters are depicted in terms of the Pearson's correlation
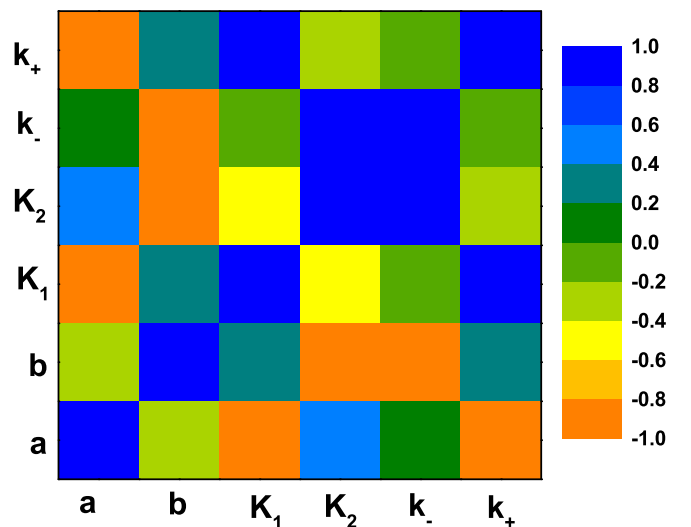

FIG. 6. The correlation among various model parameters. The values of the correlation coefficients are color coded.

TABLE III. Different properties pertaining to nuclear matter (NM) and neutron star (NS) obtained with the final parameters listed in Table II.

Type		Unit	Value
NM	ϵ_0	MeV	-15.93 ± 0.20
	ρ_0	fm^{-3}	0.1620 ± 0.003
	K_0	MeV	225.23 ± 6.38
	m_0^*/m		0.68 ± 0.04
	$m_{v,0}^*/m$		$0.78 \pm {}^{0.05}_{0.04}$
	$\Delta m_0^*/\delta$		-0.20 ± 0.09
	$C_2(\rho_0)$	MeV	33.94 ± 0.50
	L_0	MeV	68.50 ± 3.72
	K_{sym}^0	MeV	-47.46 ± 17.87
	K_τ	MeV	-349.22 ± 14.06
	M_c	MeV	998.79 ± 41.29
	Q_0	MeV	-359.23 ± 23.08
NS	$M_{\mathrm{max}}^{\mathrm{NS}}$	$M_\odot$	2.06 ± 0.03
	$R_{1.4}$	km	12.62 ± 0.57

coefficient. Two parameters are said to be fully correlated if the magnitude of the correlation coefficient for them is unity as shown by the orange and blue colors. The parameters a, K_1 and k_+ are strongly correlated among themselves; the same is true for the parameters b, K_2 and k_-. With the parameters presented in Table II the obtained fit to various macrodata are displayed by red lines in Figs. 1 and 2. One can see that the difference between the fits to the data from free variation (black line) and the calculation with the final parameters (red line) is insignificant. The isovector mass comes out to be $\frac{m_{v,0}^*}{m} = 0.78 \pm {}^{0.05}_{0.04}$.

With the parameters of the EDF as listed in Table II, the values of symmetry energy coefficient $C_2(\rho_0)$, its density slope $L_0(= 3\rho \frac{\partial C_2}{\partial \rho}|_{\rho_0})$, the curvature parameter $K_{\mathrm{sym}}^0(= 9\rho^2 \frac{\partial^2 C_2}{\partial \rho^2}|_{\rho_0})$, and the symmetry incompressibility at saturation corresponding to asymmetric nuclear matter $K_\tau(= K_{\mathrm{sym}}^0 - 6L_0 - Q_0 L_0/K_0)$ are calculated. Here, $Q_0(= 27\rho_0^3 \frac{\partial^3 \epsilon}{\partial \rho^3}|_{\rho_0})$ is the skewness parameter corresponding to SNM. Their values are listed in Table III. All of them are seen to lie within the accepted range obtained from different EDFs [9]. The value of the derivative of incompressibility $M_c(= 3\rho \frac{dK}{d\rho}|_{\rho_c})$ for SNM at a sub-saturation density $\rho_c \simeq (0.710 \pm 0.005)\rho_0$ also has excellent agreement with that obtained from examination of isoscalar giant monopole resonance (ISGMR) data for ^{208}Pb and ^{120}Sn [60,61]. For completeness, to gauge the applicability of the EDF at extremely high density, the maximum mass of the neutron star (M_{max}^{NS}) is also calculated. The EOS of the crust is taken from the Baym, Pethick, and Sutherland model [62]. The EOS of the core is calculated with the assumption of a charge-neutral uniform plasma of neutrons, protons, electrons and muons in β-equilibrium. The value of M_{max}^{NS} is seen to be $(2.06 \pm 0.03)M_\odot$, in consonance with the recently observed

maximum neutron star mass [63,64]. The value of the radius $R_{1.4}$ of a neutron star of mass $1.4M_\odot$ is also in tune with the constrained value obtained from analysis of different models [65]. In passing, it is mentioned that recently a new Skyrme EDF is proposed [66]. It is commensurate with predictions from chiral effective field theory, binding properties of finite nuclei and also the electric dipole polarizability. The effective mass is $\frac{m_0^*}{m} = 0.75 \pm 0.04$; the isovector splitting of the effective mass is positive, $\sim 0.12\delta$. However, we find it to be incompatible with the criterion for the observed maximum mass of the neutron star. The mass turns out to be $1.8M_\odot$, some what below the experimentally observed maximum mass.

IV. SUMMARY AND CONCLUSIONS

We have proposed a means of finding out the value of the nucleon effective mass m_0^* and its isovector splitting Δm_0^* by using a form of EDF [31] built without any reference to any particular interaction but with a few plausible assumptions on its nature. The structure of the EDF is seen to be equivalent to the 'standard' Skyrme functional under certain approximations. We work in the framework of this energy functional and find its parameters from χ^2-minimization of the empirical nuclear matter data and the existing 'state of the art' theoretical data pertaining to neutron matter. It is observed that the fit to these data is unable to determine m_0^* and Δm_0^* unambiguously, but yields a well-tuned combination of them; an almost indiscernible fit to the macrodata can be obtained over a wide range of their values.

From experimental data related to nuclear dipole polarizability, we show how this veil of indeterminacy can be lifted. These particular data on finite nuclei, if used judiciously give information on a linear combination of parameters determining the nucleon effective mass and its isovector splitting that is complementary to what was obtained in relation to the macrodata and thus can project out the values of the nucleon effective mass and its isovector splitting within reasonable constraints. In doing so, there is no compromise in the excellent agreement of the predicted values of the nuclear constants related to symmetric and asymmetric nuclear matter with the ones broadly accepted in present day wisdom, nor there is any sacrifice in the fit to the empirical data related to neutron stars.

[1] B. D. Serot and J. D. Walecka, Adv. Nucl. Phys. **16**, 1 (1986).

[2] L.-W. Chen, C. M. Ko, and B.-A. Li, Phys. Rev. C **76**, 054316 (2007).

[3] C. Mahaux, P. Bortignon, R. Broglia, and C. Dasso, Phys. Rep. **120**, 1 (1985).

[4] M. Jaminon and C. Mahaux, Phys. Rev. C **40**, 354 (1989).

[5] A. Bohr and B. Mottelson, *Nuclear Structure*, Vol. V. II (Benjamin, London, 1975).

[6] R. W. Hasse and P. Schuck, Phys. Lett. B **179**, 313 (1986).

[7] G. Brown and M. Rho, Nucl. Phys. A **338**, 269 (1980).

[8] L.-W. Chen, B.-J. Cai, C. M. Ko, B.-A. Li, C. Shen, and J. Xu, Phys. Rev. C **80**, 014322 (2009).

[9] M. Dutra, O. Lourenço, J. S. Sá Martins, A. Delfino, J. R. Stone, and P. D. Stevenson, Phys. Rev. C **85**, 035201 (2012).

[10] D. Davesne, J. Navarro, J. Meyer, K. Bennaceur, and A. Pastore, Phys. Rev. C **97**, 044304 (2018).

[11] B. Friedman and Pandharipande, Nucl. Phys. A **361**, 502 (1981).

[12] R. B. Wiringa, V. Fiks, and A. Fabrocini, Phys. Rev. C **38**, 1010 (1988).

[13] W. Zuo, I. Bombaci, and U. Lombardo, Phys. Rev. C **60**, 024605 (1999).

[14] Z. Zhang and L.-W. Chen, Phys. Rev. C **93**, 034335 (2016).

[15] M. Bender, P. H. Heenen, and P.-G. Reinhard, Rev. Mod. Phys. **75**, 121 (2003).

[16] J. Stone and P.-G. Reinhard, Prog. Part. Nucl. Phys. **58**, 587 (2007).

[17] X. Roca-Maza, M. Brenna, B. K. Agrawal, P. F. Bortignon, G. Colò, L.-G. Cao, N. Paar, and D. Vretenar, Phys. Rev. C **87**, 034301 (2013).

[18] X.-H. Li, W.-J. Guo, B.-A. Li, L.-W. Chen, F. J. Fattoyev, and W. G. Newton, Phys. Lett. B **743**, 408 (2015).

[19] J. Xu, L.-W. Chen, and B.-A. Li, Phys. Rev. C **91**, 014611 (2015).

[20] B. Behera, T. R. Routray, and S. K. Tripathy, J. Phys. G: Nucl. Part. Phys. **38**, 115104 (2011).

[21] J. Xu, Phys. Rev. C **91**, 037601 (2015).

[22] B.-A. Li, C. B. Das, S. Das Gupta, and C. Gale, Phys. Rev. C **69**, 011603(R) (2004).

[23] A. Burrows, S. Reddy, and T. A. Thompson, Nucl. Phys. A **777**, 356 (2006).

[24] M. Baldo, G. F. Burgio, H.-J. Schulze, and G. Taranto, Phys. Rev. C **89**, 048801 (2014).

[25] P. J. Woods and C. N. Davids, Annu. Rev. Nucl. Part. Sci. **47**, 541 (1997).

[26] G. Steigman, Int. J. Mod. Phys. E **15**, 1 (2006).

[27] H.-Y. Kong, J. Xu, L.-W. Chen, B.-A. Li, and Y.-G. Ma, Phys. Rev. C **95**, 034324 (2017).

[28] W. Zuo, L. G. Cao, B. A. Li, U. Lombardo, and C. W. Shen, Phys. Rev. C **72**, 014005 (2005).

[29] E. N. E. van Dalen, C. Fuchs, and A. Faessler, Phys. Rev. Lett. **95**, 022302 (2005).

[30] D. Bandyopadhyay, C. Samanta, S. K. Samaddar, and J. N. De, Nucl. Phys. A **511**, 1 (1990).

[31] C. Mondal, B. K. Agrawal, J. N. De, S. K. Samaddar, M. Centelles, and X. Viñas, Phys. Rev. C **96**, 021302(R) (2017).

[32] V. Baran, M. Colonna, V. Greco, and M. D. Toro, Phys. Rep. **410**, 335 (2005).

[33] R. Chen, B.-J. Cai, L.-W. Chen, B.-A. Li, X.-H. Li, and C. Xu, Phys. Rev. C **85**, 024305 (2012).

[34] R. Sellahewa and A. Rios, Phys. Rev. C **90**, 054327 (2014).

[35] L. Ou, Z. Li, Y. Zhang, and M. Liu, Phys. Lett. B **697**, 246 (2011).

[36] B. A. Brown, Phys. Rev. Lett. **111**, 232502 (2013).

[37] P. Danielewicz, W. G. Lynch, and R. Lacey, Science **298**, 1592 (2002).

[38] C. Fuchs, Prog. Part. Nucl. Phys. **56**, 1 (2006).

[39] A. F. Fantina, N. Chamel, J. M. Pearson, and S. Goriely, EPJ Web Conf. **66**, 07005 (2014).

[40] M. Prakash, T. L. Ainsworth, and J. M. Lattimer, Phys. Rev. Lett. **61**, 2518 (1988).

[41] M. B. Tsang, Y. Zhang, P. Danielewicz, M. Famiano, Z. Li, W. G. Lynch, and A. W. Steiner, Phys. Rev. Lett. **102**, 122701 (2009).

[42] M. B. Tsang, Y. Zhang, P. Danielewicz *et al.*, Int. J. Mod. Phys. E **19**, 1631 (2010).

[43] P. Danielewicz and J. Lee, Nucl. Phys. A **922**, 1 (2014).

[44] P. Russotto, S. Gannon, S. Kupny, P. Lasko, L. Acosta, M. Adamczyk, A. Al-Ajlan, M. Al-Garawi, S. Al-Homaidhi, F. Amorini *et al.*, Phys. Rev. C **94**, 034608 (2016).

[45] K. Hebeler, J. M. Lattimer, C. J. Pethick, and A. Schwenk, Astrophys. J. **773**, 11 (2013).

[46] F. Sammarruca, L. Coraggio, J. W. Holt, N. Itaco, R. Machleidt, and L. E. Marcucci, Phys. Rev. C **91**, 054311 (2015).

[47] E. Chabanat, P. Bonche, P. Haensel, J. Meyer, and R. Schaeffer, Nucl. Phys. A **627**, 710 (1997).

[48] A. Leprêtre, H. Beil, R. Bergère, P. Carlos, J. Fagot, A. D. Miniac, and A. Veyssière, Nucl. Phys. A **367**, 237 (1981).

[49] K. P. Schelhaas, J. M. Henneberg, M. Sanzone-Arenhövel, N. Wieloch-Laufenberg, and U. Z. F. Wolf, Nucl. Phys. A **489**, 189 (1988).

[50] J. Birkhan, M. Miorelli, S. Bacca, S. Bassauer, C. A. Bertulani, G. Hagen, H. Matsubara, P. von Neumann-Cosel, T. Papenbrock, N. Pietralla *et al.*, Phys. Rev. Lett. **118**, 252501 (2017).

[51] D. M. Rossi, P. Adrich, F. Aksouh, H. Alvarez-Pol, T. Aumann, J. Benlliure, M. Böhmer, K. Boretzky, E. Casarejos, M. Chartier *et al.*, Phys. Rev. Lett. **111**, 242503 (2013).

[52] T. Hashimoto, A. M. Krumbholz, P.-G. Reinhard, A. Tamii, P. von Neumann-Cosel, T. Adachi, N. Aoi, C. A. Bertulani, H. Fujita, Y. Fujita *et al.*, Phys. Rev. C **92**, 031305(R) (2015).

[53] A. Tamii, I. Poltoratska, P. von Neumann-Cosel, Y. Fujita, T. Adachi, C. A. Bertulani, J. Carter, M. Dozono, H. Fujita, K. Fujita *et al.*, Phys. Rev. Lett. **107**, 062502 (2011).

[54] O. Bohigas, A. M. Lane, and J. Martorell, Phys. Rep. **51**, 267 (1979).

[55] L. Trippa, G. Colò, and E. Vigezzi, Phys. Rev. C **77**, 061304(R) (2008).

[56] J. Dobaczewski, W. Nazarewicz, and P.-G. Reinhard, J. Phys. G: Nucl. Part. Phys. **41**, 074001 (2014).

[57] J. Erler and P.-G. Reinhard, J. Phys. G: Nucl. Part. Phys. **42**, 034026 (2015).

[58] C. Mondal, B. K. Agrawal, and J. N. De, Phys. Rev. C **92**, 024302 (2015).

[59] J. Friedrich and P.-G. Reinhard, Phys. Rev. C **33**, 335 (1986).

[60] E. Khan, J. Margueron, and I. Vidaña, Phys. Rev. Lett. **109**, 092501 (2012).

[61] E. Khan and J. Margueron, Phys. Rev. C **88**, 034319 (2013).

[62] G. Baym, C. Pethick, and P. Sutherland, Astrophys. J. **170**, 299 (1971).

[63] P. B. Demorest, T. Pennucci, S. M. Ransom, M. S. E. Roberts, and J. W. T. Hessels, Nature **467**, 1081 (2010).

[64] J. Antoniadis *et al.*, Science **340**, 1233232 (2013).

[65] J. M. Lattimer and Y. Lim, Astrophys. J. **771**, 51 (2013).

[66] Z. Zhang, Y. Lim, J. W. Holt, and C. M. Ko, Phys. Lett. B **777**, 73 (2018).